

RESEARCH ARTICLE

Disambiguation of Uniform Demagnetization Fault From Position Sensor Fault in FOC PMSM Applications

SANDUN S. KURUPPU¹, (Senior Member, IEEE),

AND SUNIL G. ABEYRATNE², (Senior Member, IEEE)

¹Department of Electrical and Computer Engineering, Saginaw Valley State University, University Center, MI 48710, USA

²Department of Electrical and Electronics Engineering, University of Peradeniya, Peradeniya 20400, Sri Lanka

Corresponding author: Sandun S. Kuruppu (skuruppu@svsu.edu)

This work was supported in part by the Ruth and Ted Braun Fellowship.

ABSTRACT Electrification of higher torque density applications in the transportation sector and robotics sector are primarily met with permanent magnet synchronous machines (PMSMs), attributing to their unique properties. However, wide operating temperatures, field weakening controls, and low-quality magnets, lead to uniform demagnetization of rotor magnets. Demagnetization in torque control applications reduce the effective output torque as the output torque is proportional to rotor flux level. Detection of such rotor demagnetization is essential and only second to few key faults from the system perspective. However, static position sensor offset error (SPSOE) is a fault mode that may mask itself as a demagnetization fault. Though the demagnetization fault is irreversible, the SPSOE is remediable avoiding sustained-severe degradation of system performance. The false positive nature of demagnetization detection and the SPSOE are discussed in detail in the paper, and a disambiguation strategy is proposed and successfully implemented. Simulation and experimental results are presented to validate the effectiveness of the proposed strategy.

INDEX TERMS Demagnetization diagnosis, fault detection, fault disambiguation, machine vector control, permanent magnet synchronous motors, position measurement.

I. INTRODUCTION

Electrification in the transportation sector has outgrown the powertrain and into many other subsystems. Historically, transition to an electromechanical energy conversion system was driven by efficiency. However, more recently the ease of interfacing with artificial intelligence (AI) has become another advantage. With the success of electrification in the ground transportation sector, the next leap is to address efficiency and reliability challenges in the aerospace industry through electrification. Ground as well as aerospace transportation application subsystems such as propulsion/powertrain, steering, power generation, thermal management and air conditioning systems are being converted to electric. Numerous other industries such as robotics,

manufacturing and consumer products are also rapidly growing in size, fueled by the mechatronic systems integrated with AI. Among the machines popular for electromechanical energy conversion, permanent magnet synchronous machines (PMSMs) have proven to be advantageous. Despite the cost of rare earth magnets, the higher torque density, compact design, better thermal characteristics, and simple, high dynamic control have become the factors favoring PMSMs.

Electric machines used in powertrain, aerospace propulsion, power generation units, and steering systems are subjected to high temperature conditions, high currents and field weakening control to achieve higher speeds without increasing the DC link voltage. Field weakening enables PMSMs to operate at higher speeds without sacrificing their high torque capability at low speed. However, subjecting a PMSM to high temperatures and field weakening for a prolonged period, demagnetizes the rotor magnets

The associate editor coordinating the review of this manuscript and approving it for publication was Feifei Bu¹.

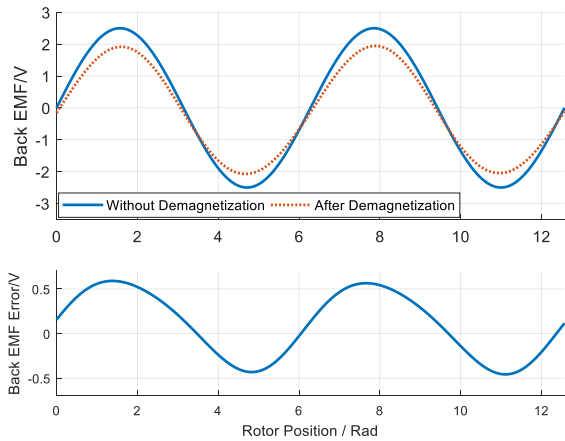


FIGURE 1. Induced EMF profile example under non-uniform demagnetization at constant speed.

to a certain degree [1], [2], [3]. Additionally, manufacturing defects may also contribute to accelerating the demagnetization process [4].

The key contribution of this paper stems from the fact that accurate demagnetization detection is overshadowed by another critical fault, a static position sensor offset error (SPSOE).

An SPSOE has the potential to falsely trigger demagnetization detection algorithms. Both demagnetization fault and SPSOE faults degrade system performance, while an SPSOE has much more severe consequences from a system point of view. Disambiguation of the two faults is of paramount importance because, even though demagnetization fault cannot be remedied, an SPSOE can be compensated, restoring the system to return to optimal performance.

With all magnets on the rotor being subjected to field weakening, uniform demagnetization effect can be represented by a significant reduction in the fundamental flux linkage and added harmonic content on flux linkage constant (λ_m^r is the flux linkage constant)

Demagnetization is easily observed through induced electromotive force (Induced EMF or back EMF) profile of a machine as the induced EMF is a function of speed and flux linkage (1). Figure 1 illustrates an example of how demagnetization may be represented by induced EMF at a constant speed.

$$E_{as}(\theta_r) = E \sin(\theta_r + \varphi_1) + e_0 + \sum_{k=2}^{\infty} e_k \sin(k\theta_r + \varphi_k) \quad (1)$$

E_{as} is phase A back electromotive force (induced EMF), which is represented as a function of θ_r , the rotor position of the motor. E is the magnitude of the fundamental component in the induced EMF signal. k , e_k , and φ_k are integer representing harmonic order, magnitude of the k^{th} induced EMF component and phase of k^{th} induced EMF component, respectively.

In this scenario a uniform demagnetization effect is considered as all magnets on the rotor are subjected to the opposing

flux generated by the stator used for field weakening. Therefore, it is assumed that the flux linkage coefficient is reduced introducing a reduction in the induced EMF amplitude as in (2). The DC offset (e_0) and the higher order harmonics are assumed to be negligible during the considered uniform demagnetization scenario. $\hat{\lambda}_m^r$ is the flux linkage constant amplitude after demagnetization.

$$E_{as}(\theta_r) = \hat{\lambda}_m^r \omega_r \sin(\theta_r) \approx \lambda_m^r \omega_r \sin(\theta_r) - \Delta \lambda_m^r \omega_r \sin(\theta_r) \quad (2)$$

where, ω_r represents the motor speed. Reduced flux linkage constant implies that the machines torque constant has also reduced, resulting in lower torque output at the same regulated current in torque-controlled applications. In speed-control applications, the higher currents injected by the controller increases the system losses leading to elevated operating temperatures, promoting demagnetization. Therefore, detecting significant amount of uniform demagnetization is essential to sustain system performance. Uniform demagnetization detection in applications is achieved through several different strategies [1], [2], [3], [4], [5]. Among them, the quadrature axis voltage measurement is a common approach in industry. However, this method results in a false positive under static position sensor offset error (PSOE), which is a severe fault by itself. Due to symmetric nature of uniform demagnetization and PSOE, a proper disambiguation strategy needs to be devised. This paper presents a strategy to cohesively disambiguate between uniform demagnetization and PSOE through model-based signature analysis.

The organization of the paper is as follows. Introductory section states the problem and summarizes the existing body of work on demagnetization detection. More importantly, their inability to distinguishing a PSOE presented. Section II through IV explains how the false-positive may occur in the demagnetization detection strategy. A detailed analysis has been provided and the phenomenon is illustrated through simulation and experimental results. Particularly, section III provides experimental and simulation results and section IV details the demagnetization detection algorithm. Sections V and VI cover the disambiguation strategy and present the analysis, simulation, and experimental results. Particularly, section V discusses how the PSOE causes false positives in demagnetization detection algorithm and proposes a disambiguation strategy. Section VI concludes the paper with final remarks.

Demagnetization detection in PMSMs have been studied by number of researchers and are discussed here to emphasize the significance of the research presented in this paper. The focus of this paper is to disambiguate between PSOE and uniform demagnetization through a signal analysis-based approach. Therefore, finite element analysis (FEA) of motor demagnetization is not considered in this body of work. To provide a comprehensive analysis, we have cited references that include FEA results under demagnetization faults. The authors of [5] propose a real-time demagnetization

assessment method for PMSMs based on a transfer inductance matrix. The demagnetization assessment is made based on a first order approximation of the demagnetization characteristics under varying parameter levels such as current references, resulting in a temperature estimate. Zhao *et al.* in [6] propose an adaptive linear neuron model reference adaptive system for uniform demagnetization detection in a linear PMSM through flux linkage observation. A Series of demagnetizations are considered for model evaluation under different speeds, in a speed-controlled application. Three different algorithms are also compared for their accuracy. However, the complexity of these proposed algorithms renders them impractical for many applications. An α - β subspace harmonic mapping based uniform demagnetization detection in PMSM is proposed in [7]. The authors propose 5th harmonic component as a means to detect uniform rotor magnet demagnetization in six phase surface mount PMSMs. A search coil-based winding failure and demagnetization detection is proposed in [8]. However, the results are only based on finite element analysis. Hong *et al.* in [9] propose a strategy to detect PMSM rotor faults using a test embedded in the inverter to be used when the machine is not in operation. The approach is using a signal injected through the d-axis current to classify and identify faults. Typically, such off-state testing is not conducted in consumer applications such as automotive due to safety concerns and prevents the detection of a fault that occurred during normal operation (during run time). Frequency domain approaches such as wavelet-based fault detection has been widely proposed for demagnetization diagnosis in [10], [11], [12], and [13]. Asymmetric magnet fault detection using leakage flux is proposed in [14]. A fluxgate sensor, which is a special type of sensor is used to measure leakage which are otherwise difficult to measure. Harmonic content visible on the leakage flux spectra are used to detect these asymmetric magnet failure modes such as broken magnets. Zhu *et al.* proposes a flux based acoustic noise model for demagnetization and a back propagation neural network to detect demagnetization based on acoustic data. The authors claim that the method is computationally efficient and not sensitive to machine parameters [15], [16]. However, it is not clear how authors justify the claims as machine parameters vary in a mass-manufacturing environment causing the harmonic amplitudes to change. Further, frequency domain spectrum generation requires high computational power, which may not be available on consumer applications. Authors of [17] and [18] propose search coil-based approaches for rotor demagnetization detection. These approaches, similar to other embedded-sensor-based approaches, require unique motor designs or motor modifications. A stator tooth flux based online demagnetization detection is discussed in [19]. A convolutional neural network combined with frequency domain motor current signatures are considered in [20] to detect damage to permanent magnets in a PMSMs. [1] presents a summary of available techniques and emphasizes the difficulty in detecting uniform

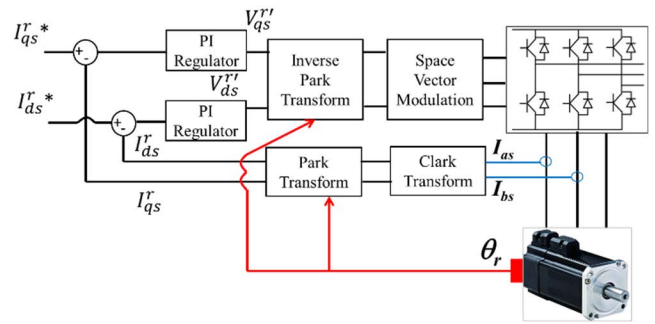


FIGURE 2. Field oriented control algorithm block diagram considered.

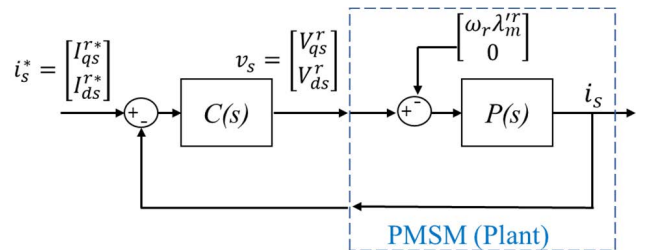


FIGURE 3. Simplified block diagram of field-oriented control algorithm with position sensor.

demagnetization through motor current signature analysis. Frequency domain harmonics maybe caused by other types of faults too. More notably methods in existing literature fail to identify how a static position offset error results in a false positive demagnetization fault, if not properly distinguished. Hence this paper proposes a uniform demagnetization strategy using real-time signals along with a disambiguation strategy from position sensor offset error fault. The proposed approach is for a sensed (uses a position sensor to measure rotor position) field-oriented controlled (FOC) PMSM used in a torque control application. References [5], [9], [10], and [12] provide a comprehensive overview of FEA based results related to PMSM demagnetization for the interested reader.

II. DISCUSSION ON DEMAGNETIZATION DETECTION AND QUANTIFICATION VIA LINEAR PMSM MODEL

A field oriented controlled PMSM system block diagram in a torque-controlled application is shown in figure 2. The dynamic model, voltage equations of a PMSM in rotor reference frame are given in (3) and (4). A position sensor is used to measure rotor position and orient stator flux for optimal torque generation. Proportional and integral regulators (PI regulators) are used to maintain the required currents based on torque demand.

$$V_{qs}^r = L_q \frac{di_{qs}^r}{dt} + r_s i_{qs}^r + \omega_r L_d i_{ds}^r + \omega_r \lambda_m^r \quad (3)$$

$$V_{ds}^r = L_d \frac{di_{ds}^r}{dt} + r_s i_{ds}^r - \omega_r L_q i_{qs}^r \quad (4)$$

V_{qs}^r , V_{ds}^r , i_{qs}^r and i_{ds}^r are q-axis voltage, d-axis voltage, q-axis current and d-axis current respectively. L_q , and L_d , are inductances along each axis while r_s and ω_r represent resistance and rotor speed, respectively.

For the purpose of analysis, the FOC system may be viewed as a two state, state-space representation in matrix form. Assuming the position sensor offset is accurately calibrated, and the inverter is a linear plant of unity gain, the system block diagram for the proposed representation is as follows.

I_{qs}^{r*} and I_{ds}^{r*} represent rotor reference frame current references applied to the FOC algorithm. K_P , K_I and s are proportional gain, integral gain and Laplace variable, respectively. $C(s)$ and $P(s)$ are as follows,

$$C(s) = \begin{bmatrix} (K_P s + K_I)/s & 0 \\ 0 & (K_P s + K_I)/s \end{bmatrix} \quad (5)$$

$$P(s) = \begin{bmatrix} r_s + sL_q & \omega_r L_d \\ -\omega_r L_q & r_s + sL_d \end{bmatrix}^{-1} \quad (6)$$

$C(s)$ represents PI regulators while $P(s)$ represent the motor represented in rotor reference frame for analysis. K_P and K_I values were chosen to modify closed loop system bandwidth to desired values by cancelling plant poles. K_I was chosen as $\omega_{BW} L_q$ and K_P was chosen as $\omega_{BW} r_s$, where the closed loop system bandwidth (ω_{BW}). The effect of the demagnetization is screened strategically using the voltage applied to the motor (v_s). The following closed loop transfer function may be obtained for the above system shown in figure 3.

$$\begin{bmatrix} V_{qs}^r \\ V_{ds}^r \end{bmatrix} = \frac{C(s)}{[I + C(s)P(s)]} \begin{bmatrix} I_{qs}^{r*} \\ I_{ds}^{r*} \end{bmatrix} + \frac{C(s)P(s)}{[I + C(s)P(s)]} \begin{bmatrix} \omega_r \lambda_m^{\prime r} \\ 0 \end{bmatrix} \quad (7)$$

Considering the step input response of a healthy system (i.e., no uniform demagnetization) at steady state, the above relation reduces to (8).

$$\begin{bmatrix} V_{qs}^r \\ V_{ds}^r \end{bmatrix} = \begin{bmatrix} r_s & \omega_r L_d \\ -\omega_r L_q & r_s \end{bmatrix} \begin{bmatrix} I_{qs}^{r*} \\ I_{ds}^{r*} \end{bmatrix} + \begin{bmatrix} 1 & 0 \\ 0 & 1 \end{bmatrix} \begin{bmatrix} \omega_r \lambda_m^{\prime r} \\ 0 \end{bmatrix} \quad (8)$$

However, in the situation where uniform demagnetization has occurred, the rotor reference frame voltages applied to the motor are given by (9). Note that true motor currents are considered in (9) assuming PI regulators are properly regulating the requested current references. It is evident that with uniform demagnetization, the applied q-axis voltage reduces. $V_{qs_m}^r$ and $V_{ds_m}^r$ represent the rotor reference frame voltage generated by the PI regulators that are applied to the motor via the inverter. These values are available in the controller itself and no additional measurement or calculation is needed. (9) is provided to demonstrate the relationship between rotor reference frame voltages and demagnetized

magnets (uniform demagnetization).

$$\begin{bmatrix} V_{qs_m}^r \\ V_{ds_m}^r \end{bmatrix} = \begin{bmatrix} r_s & \omega_r L_d \\ -\omega_r L_q & r_s \end{bmatrix} \begin{bmatrix} I_{qs}^r \\ I_{ds}^r \end{bmatrix} + \begin{bmatrix} 1 & 0 \\ 0 & 1 \end{bmatrix} \begin{bmatrix} \omega_r \hat{\lambda}_m^{\prime r} \\ 0 \end{bmatrix} \quad (9)$$

Rotor reference frame voltages shown in (8) can be calculated given the motor parameters, motor speed and reference currents. The difference between the voltages applied to the motor and the voltages computed based on the model will emphasize the voltage difference induced by the demagnetization as in (10). These voltage errors are represented by $V_{qs_err}^r$ and $V_{ds_err}^r$.

$$\begin{bmatrix} V_{qs_err}^r \\ V_{ds_err}^r \end{bmatrix} = \begin{bmatrix} V_{qs}^r - V_{qs_m}^r \\ V_{ds}^r - V_{ds_m}^r \end{bmatrix} = \begin{bmatrix} \omega_r (\lambda_m^{\prime r} - \hat{\lambda}_m^{\prime r}) \\ 0 \end{bmatrix} \quad (10)$$

$$V_{qs_err}^r / \omega_r = \lambda_m^{\prime r} - \hat{\lambda}_m^{\prime r} \quad (11)$$

Speed normalized quadrature axis voltage error as shown in (11), indicates the error in flux linkage constant. In practical applications, machines tend to operate outside magnetically linear region causing the flux linkage constant to change, causing a false positive demagnetization fault. A sufficiently accurate flux linkage coefficient profile as a function of machine current during calibration phase will eliminate such false positives. The following section provides simulation and experimental results for the uniform demagnetization diagnosis approach.

III. SIMULATION AND EXPERIMENTAL RESULTS OF DEMAGNETIZATION FAULT BEHAVIOR

A. SIMULATION RESULTS

Prior to experimental validation, MATLAB Simulink based simulations were conducted to validate the proposed strategy. The system used for the simulation study closely models the experimental setup to be discussed in part b, below. The PMSM is operated in torque control mode, while the mechanical system speed is maintained constant by a dynamometer.

Figure 4 illustrates the effect of varying uniform demagnetization on rotor reference frame voltage errors discussed in (10). Simulations results in figure 4 are at varying uniform demagnetization levels, while the speed is held constant. Simulation data was collected under six different speed settings. First subplot depicts the quadrature axis current which is regulated at 1 A. Second subplot is representing the variation of flux linkage coefficient, at each level of demagnetization. Third and fourth subplots indicate the behavior of the rotor reference frame voltage errors at each operating condition (as in (10)). The results clearly show that increased demagnetization under torque control operation has an influence on $V_{qs_err}^r$ in the steady state but no effect on $V_{ds_err}^r$. This reveals the important result that a uniform demagnetization effect only reflects on the quadrature axis voltage, and that it has no effect on the direct axis voltage.

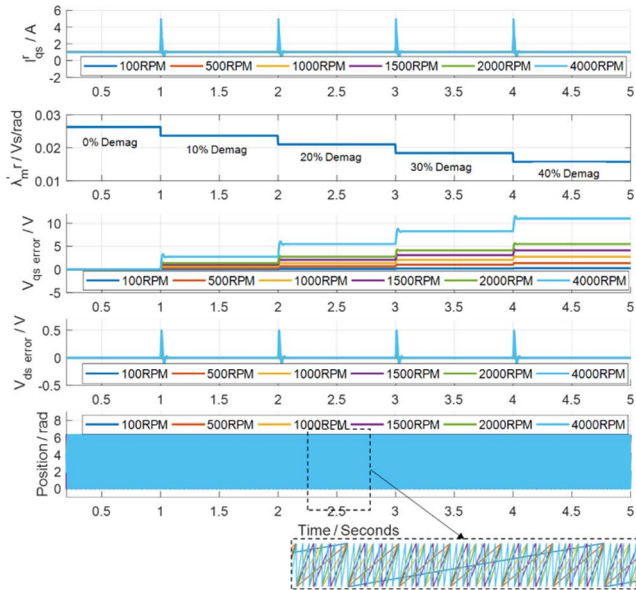


FIGURE 4. Uniform demagnetization detection error with varying speed.

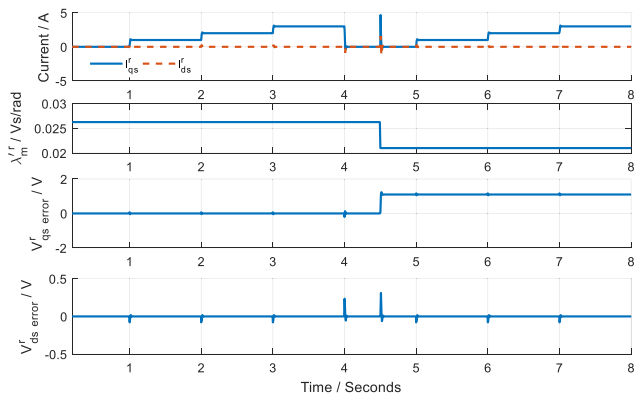


FIGURE 5. Uniform demagnetization detection error with varying current.

The transients visible in the current and voltage plots are caused by the closed loop system response to the introduced demagnetization and regulating current at the intended reference value. Simulation results in figure 4 justify the relation obtained in analysis, demonstrating the proportional increase of quadrature axis voltage error, along with increasing demagnetization.

Figure 5 illustrates the response of rotor reference frame voltage errors with varying quadrature axis current reference while the speed and the demagnetization level are maintained constant. As seen in the first subplot of figure 5, the quadrature axis current is increased in steps of 1 A. Direct axis current is regulated to be at 0 A. The second subplot shows the variation in flux linkage coefficient (i.e., demagnetization level). A 20% demagnetization is introduced at $t = 4.5$ seconds. Motor speed is maintained constant at 2000 RPM during this test. Simulation results shown in figure 5 conclude that there is no influence of motor current on the proposed demagnetization detection scheme.

TABLE 1. PMSM parameters.

Parameter	Value
Poles	10
Rated voltage	42 V
Phase Resistance (r_s)	0.2239 Ω
Q-axis Inductance (L_q)	367.2 μH
Flux Linkage Constant (λ_m^r)	0.0122 V/(rads ⁻¹)

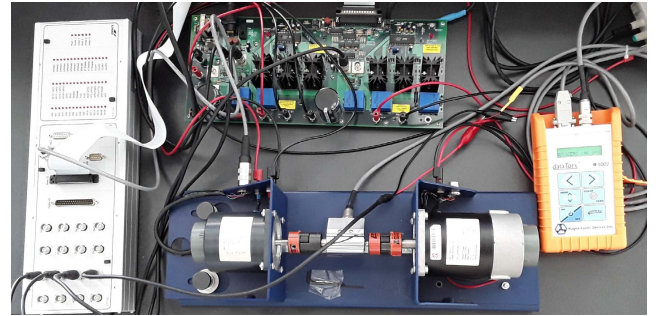


FIGURE 6. PMSM demagnetization algorithm validation setup with torque sensor.

B. EXPERIMENTAL RESULTS

Experimental validation of the proposed method is presented here. The experimental setup is depicted in figure 6 followed by the parameters of the PMSM in Table 1. The PMSM is coupled to a DC machine through an in-line torque sensor. Both machines are controlled with dSPACE DS1104 R&D platform shown. The PMSM is operated in field oriented controlled torque mode, whereas the DC machine is speed regulated. The demagnetization detection as well as the demagnetization effect emulation was also implemented on the same dSPACE platform. dSPACE systems is a rapid prototyping platform facilitated by Matlab Simulink based auto coding. The underlying DSP is a MPC8240 processor with PPC 603e core operating at 250 MHz clock.

According to (11), under uniform demagnetization, $\hat{\lambda}_m^r < \lambda_m^r$. Therefore, $V_{qs_m}^r < V_{qs}^r$. V_{qs}^r is a computed value based on motor parameters, current references and motor speed, according to (8) to be compared with the applied voltage in rotor reference frame, which is $V_{qs_m}^r$. However, demagnetizing a machine is permanent and makes the machine useless for future research. Hence, for the purpose of algorithm validation, uniform demagnetization was emulated by achieving $V_{qs_m}^r < V_{qs}^r$ condition through modifying the λ_m^r value to be larger than the nominal value. For dynamometer testing, this was deemed acceptable as the faulty motor is acting as the torque regulator and the dynamometer (DC motor) is regulating speed, which matches the torque on the faulty PMSM.

Figure 7 through 9 depict experimental results on how the emulated uniform demagnetization effect is reflected on the quadrature and direct axis voltage error. Since uniform demagnetization of a PMSM is permanent, and renders the machine unusable, characteristics similar to demagnetization was emulated based on the result in (10). Under a uniform demagnetization effect, the flux linkage coefficient changes

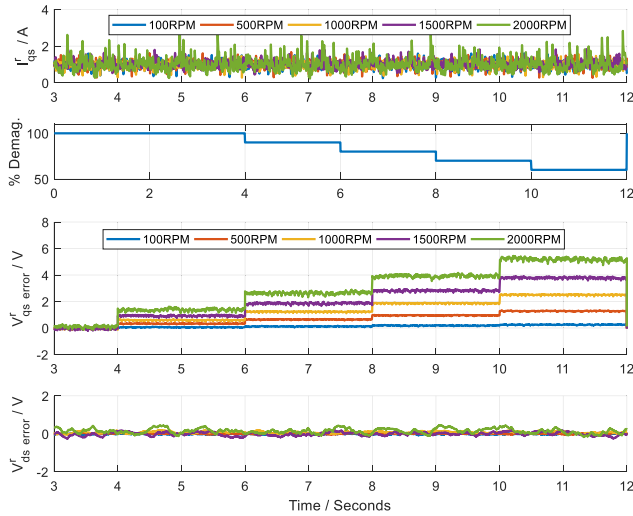


FIGURE 7. Rotor reference frame voltage error variation at different emulated demagnetization levels with varying speed.

from λ_m^r to $\hat{\lambda}_m^r$. Therefore, to evaluate the proposed algorithm and the disambiguation strategy, the flux linkage coefficient used by the rotor reference frame (RRF) voltage error calculation was varied. In doing so, the proposed algorithm experiences an effect similar to a uniform demagnetization, allowing for algorithm development without permanently demagnetizing the PMSM.

Figure 7 depicts the variation of RRF voltages under different emulated demagnetization conditions and varying speeds. For each test, the speed was maintained constant while the demagnetization level is increased from 0% to 40% in increments of 10%. PMSM current reference was maintained constant with $I_{qs}^{r*} = 1A$ and $I_{ds}^{r*} = 0 A$ (subplot 1). Second subplot represents the level of demagnetization. Third and fourth subplots are for $V_{qs_err}^r$, $V_{ds_err}^r$, respectively. The q-axis voltage errors follow (11), showing that increasing speed results in higher voltage error for uniform demagnetization detection. No significant variation is observed on the direct axis voltage error. Hence it is experimentally verified that a uniform demagnetization has a direct influence on q-axis voltage only.

The effect of varying current reference under two different demagnetization scenarios are studied in figure 8 as increasing stator current results in more airgap flux. The speed of the PMSM was maintained at 500 RPM, while the current reference was changed from 0A to 3.5 A in steps of 0.5 A. First subplot of figure 8 show the regulated motor current. Second and third subfigures, depict the variation of RRF voltage errors. Unlike simulations, the quadrature axis voltage error (Figure 8 second subplot) shows a slight variation due to the varying current references. This is primarily due to the level of air gap flux changing with changing current reference and non-linear saturation characteristics. The simulation assumes an ideal machine and therefore does not demonstrate a similar effect. A simple look up table-based voltage error compensation strategy was implemented to correct for the error introduced by magnetic non-linearities at varying cur-

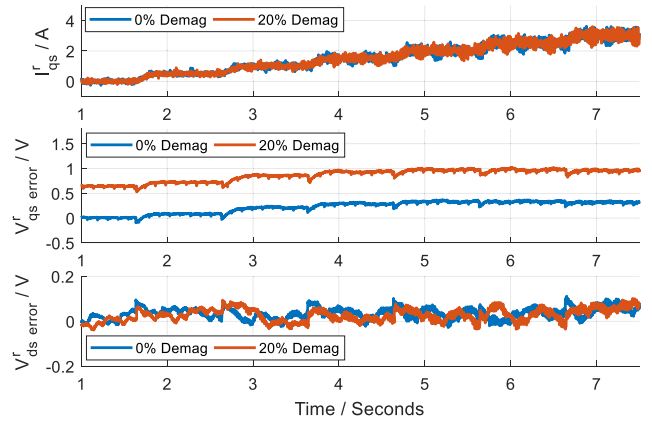


FIGURE 8. Rotor reference frame voltage error variation at different emulated demagnetization levels with varying current references at 500RPM. (Without non-linearity compensation.)

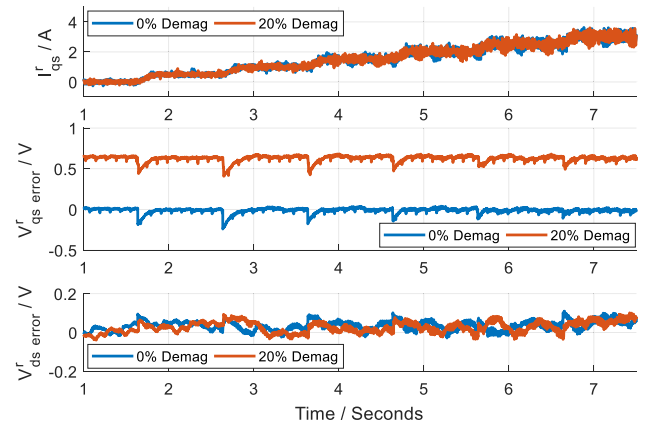


FIGURE 9. Rotor reference frame voltage error variation at different emulated demagnetization levels with varying current references at 500 RPM (with current reference based non-linearity compensation).

rent levels. The look-up table implementation is shown in figure 10.

The reference current used by the FOC algorithm was used as the input to the look up table to prevent additional noise from influencing the demagnetization detection algorithm. Results after the current based compensation are shown in figure 9. It is evident that the results with current based compensation show no variation of voltage error with varying current.

The updated uniform demagnetization detection algorithm is provided in the block diagram below (Figure 10). The block diagram also includes transient blocking and a threshold compared with q-axis voltage error to trigger a uniform demagnetization fault flag. The transient blocking filter bandwidth has been set to 10% of the current regular bandwidth, which is 100 rads^{-1} in this experiment. The fault trigger threshold has been set to detect a demagnetization of 5% or more. Since the voltage error is normalized with respect to speed and λ_m^r the quantity compared with the fault threshold is the amount of change in uniform demagnetization. Simulation results and experimental results under varying conditions are discussed in the next section.

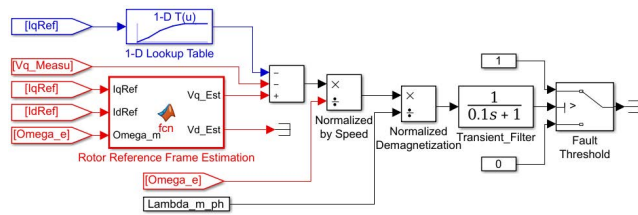


FIGURE 10. Implementation of the proposed demagnetization detection method.

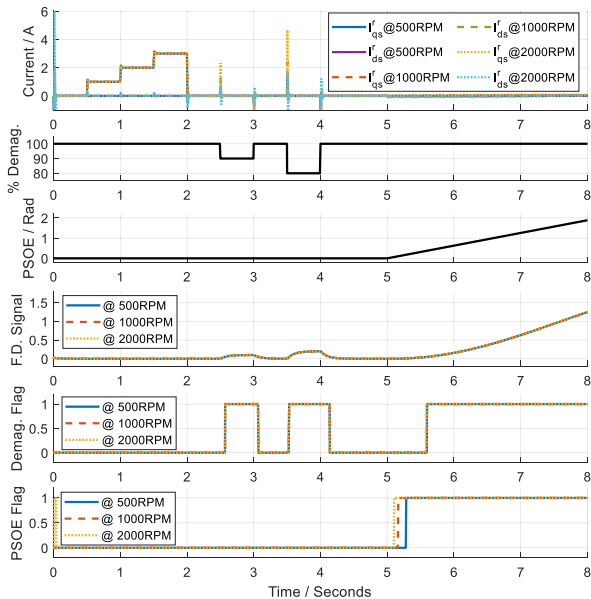


FIGURE 11. Simulation results of the proposed demagnetization detection method at varying currents and speeds.

IV. SIMULATION AND EXPERIMENTAL RESULTS OF DEMAGNETIZATION DETECTION

Characteristics of the demagnetization detection algorithm is presented under different scenarios to demonstrate the behavior under transient states. Figure 11 illustrates simulation results at different operating points, with uniform demagnetization fault being injected between $t = 2$ seconds to $t = 4$ seconds. From $t = 0$ seconds to $t = 2$ seconds, the current reference is being changed to illustrate that there is no false positive caused by current transients in the demagnetization detection algorithm. The results shown after $t > 4.5$ seconds illustrate how position sensor offset error (PSOE) influences the fault diagnosis system and this will be discussed in the next section, as it relates to the false positive causes and disambiguation. Fourth subplot in figure 11 depicts the normalized uniform demagnetization signal with 5th and 6th subplots being fault detection flags for uniform demagnetization and disambiguation, respectively. Results in figure 11 demonstrate the fact that the demagnetization detection flag is immune to changes in the current reference. Thus, the result displays the robustness of uniform demagnetization detection towards current reference changes, while demonstrating how a PSOE poses the threat of a false positive.

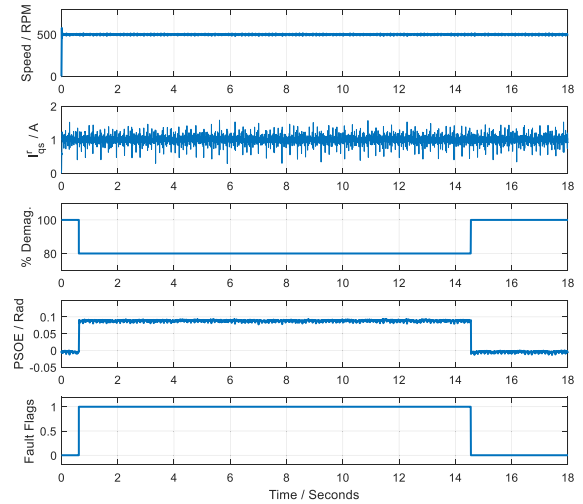


FIGURE 12. Experimental implementation results of the rotor reference frame-based demagnetization detection method.

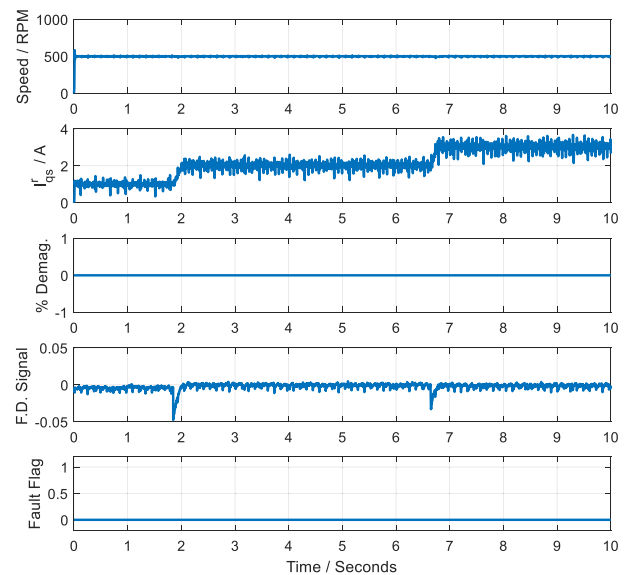


FIGURE 13. Current transient handling of the demagnetization detection method.

Figure 12 is an experimental validation of the demagnetization detection scheme discussed above. A 20% uniform demagnetization is introduced at 500RPM and 1A of quadrature axis current. The fault diagnosis signal (F.D. Signal in fourth subplot) is experiencing an increase, followed by the Fault flag being set (fifth subplot). The flag and the F.D. signal subside, immediately after the demagnetization fault is removed, concluding that the demagnetization detection is functional under a demagnetization fault.

Figure 13 experimentally evaluates to see if current transients cause any false positives in the proposed fault diagnosis approach. At 500 RPM, the current reference is being changed from 1 A to 2 A and then to 3 A. Despite the transients in the F.D. signal, the threshold and filtering used in the proposed algorithm help mitigate potential false positives caused by current transients.

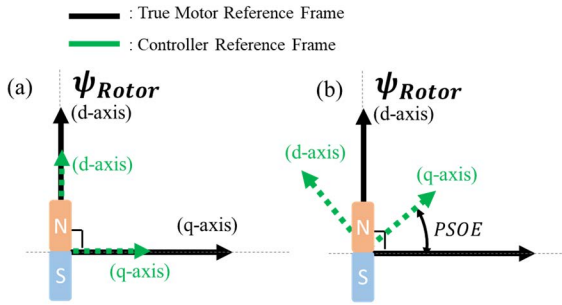


FIGURE 14. Comparison of rotor reference frame alignment with and without PSOE. (a) without PSOE, (b) with PSOE.

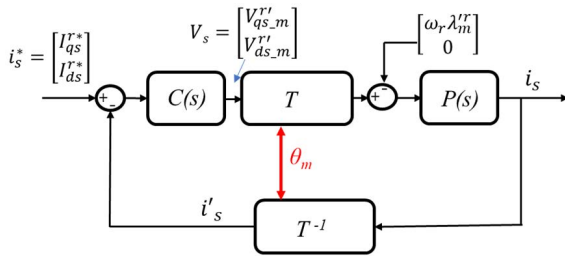


FIGURE 15. Effect of PSOE on signals used for demagnetization detection.

Both simulation and experimental result shown above validate the capability of the demagnetization detection strategy to identify uniform demagnetization. However, there is a potential source of false positive that need to be addressed. This is discussed in the next section.

V. EFFECT OF PSOE ON DEMAGNETIZATION DETECTION AND DISAMBIGUATION STRATEGIES

This section demonstrates how a PSOE may influence demagnetization detection strategy adversely, followed by an explanation on how this may be mitigated through a disambiguation signal. Step by step experimental results are provided on how the disambiguation process functions.

A position sensor offset error essentially shifts the controller reference frame away from the true rotor reference frame. Figure 14. (a) depicts a properly aligned controller reference frame whereas figure 14. (b) shows a misaligned controller reference frame. Despite the shift in alignment between true motor reference frame and the controller reference frame, current regulators continue to regulate current in this incorrect reference frame resulting in currents in the true motor reference frame to change (ex: d-axis current injected to the motor when controller assumes d-axis current is zero, or negative q-axis current injected to the motor while controller assumes positive q-axis current is being injected.) The controller reference frame misalignment due to PSOE is modelled as a transformation that varies with PSOE as shown in Fig. 14(a). Hence the resulting new current regulated system is depicted in the block diagram shown in figure 15.

$$T = K_s(\theta_r) K'_s(\theta_e) = \begin{bmatrix} \cos(\theta_r - \theta_e) & -\sin(\theta_r - \theta_e) \\ \sin(\theta_r - \theta_e) & \cos(\theta_r - \theta_e) \end{bmatrix} \quad (12)$$

$$K_s = \frac{2}{3} \begin{bmatrix} \cos(\theta) \cos(\theta - 2\pi/3) \cos(\theta + 2\pi/3) \\ \sin(\theta) \sin(\theta - 2\pi/3) \sin(\theta + 2\pi/3) \end{bmatrix} \quad (13)$$

$$K'_s = \begin{bmatrix} \cos(\theta) & \sin(\theta) \\ \cos(\theta - 2\pi/3) & \sin(\theta - 2\pi/3) \\ \cos(\theta + 2\pi/3) & \sin(\theta + 2\pi/3) \end{bmatrix} \quad (14)$$

θ_r and θ_e are true motor rotor position and measured rotor position respectively. K_s is the forward reference frame transformation and K'_s is the inverse reference frame transformation. The resulting closed loop system transfer function due to PSOE under dynamic conditions is represented by (15).

$$v'_s = \frac{C(s)}{[I + C(s)T^{-1}P(s)T]} i_s^* + \frac{C(s)T^{-1}P(s)}{[I + C(s)T^{-1}P(s)T]} e_s \quad (15)$$

The above result maybe further reduced by considering the steady state response of the system for a step input (I/s), resulting in (16) and (17) shown below. $i_s^* = [I_{qs}^* I_{ds}^*]^T$.

$$\begin{bmatrix} V_{qs_m}^r \\ V_{ds_m}^r \end{bmatrix} = \begin{bmatrix} r_s & \omega_r L_d \\ -\omega_r L_q & r_s \end{bmatrix} \begin{bmatrix} I_{qs}^{r*} \\ I_{ds}^{r*} \end{bmatrix} + \begin{bmatrix} \cos(\Delta\theta) \\ -\sin(\Delta\theta) \end{bmatrix} \omega_r \lambda'_m \quad (16)$$

$$\begin{bmatrix} V_{qs_err}^r \\ V_{ds_err}^r \end{bmatrix} = \begin{bmatrix} V_{qs}^r - V_{qs_m}^r \\ V_{ds}^r - V_{ds_m}^r \end{bmatrix} = \begin{bmatrix} -\cos(\Delta\theta) \\ \sin(\Delta\theta) \end{bmatrix} \omega_r \lambda'_m \quad (17)$$

Above result concludes that PSOE has direct influence on q-axis voltage, d-axis voltage, and voltage error terms that are used for uniform demagnetization detection.

To summarize, as shown in figure 16, uniform demagnetization only affects q-axis voltage equation. However, PSOE effects both q- and d- axis voltage equations (from a motor point of view). Hence, we show that $V_{qs_err}^r$ is affected by both uniform demagnetization fault and PSOE. But $V_{ds_err}^r$ is only affected by PSOE. FOC controlled PMSMs require rotor position information for optimal stator field orientation and commutation. However, as discussed in [21], [22], and [23], position sensor measurement may contain a DC offset (PSOE: position sensor offset error) and/or harmonic content. Of these, the PSOE has a significant impact on system torque output, along with the potential to cause a false positive in demagnetization detection approach(s). Experimental result below supports the above argument. Figure 17 illustrates the behavior of $V_{qs_err}^r$ and $V_{ds_err}^r$ discussed in (10) and (17) during a varying PSOE at different speeds. The varying PSOE value is shown in the first subplot of figure 17. The effect is only amplified at higher speed as seen by the increasing voltage error amplitudes in subplot 3 and 4. As discussed next this characteristic serves as a means to disambiguate the two faults.

The effect of PSOE on the uniform demagnetization detection method is shown in figures 11 (simulation) and 18

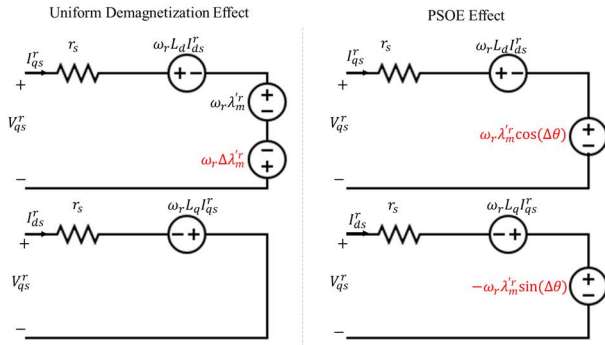


FIGURE 16. Difference between PSOE and uniform demagnetization effect from a voltage equation point of view.

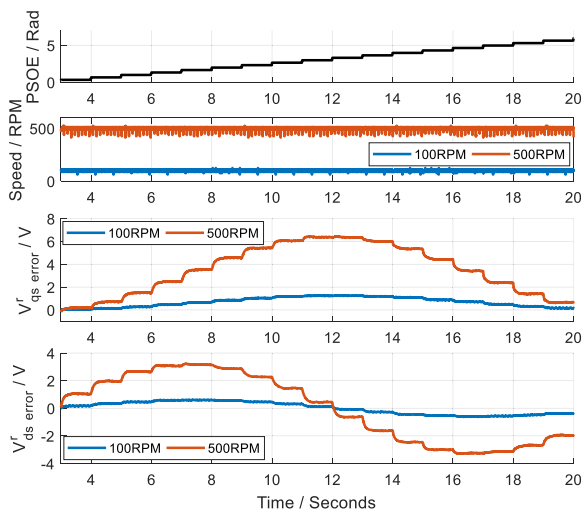


FIGURE 17. Effect of PSOE on signals used for demagnetization detection.

(experimental). Motor speed is maintained at 500RPM, and the current is regulated at 1 A. The demagnetization percentage is held at 0% while a PSOE is being injected to the system artificially. The PSOE, as shown in fourth subplot, is being varied from zero to 2π radians in steps of 0.331 radians. The fifth subplot is the uniform demagnetization fault diagnosis signal ($V^r_{qs_err}$), followed by the uniform demagnetization detection flag in the 6th subplot. Since demagnetization fault and PSOE cause the $V^r_{qs_err}$ to rise, a disambiguation strategy is needed to identify the two faults independently. The primary difference between the two faults is that the PSOE gives rise to $V^r_{ds_err}$ whereas a uniform demagnetization has no effect on this signal. Therefore, a second fault flag is generated based on $V^r_{ds_err}$ signal deviation from a threshold voltage, to disambiguate between the two faults. The threshold for fault flag was chosen to be 0.2 V of d-axis voltage error which translates to 0.3radians of PSOE. The threshold selection for PSOE detection uses the following formula.

$$V_{err_Threshold} = \sin(\Delta\theta) \omega_r \lambda'_m \quad (18)$$

The disambiguation flag implementation is shown in the proposed addition in figure 19 and the fault disambiguation

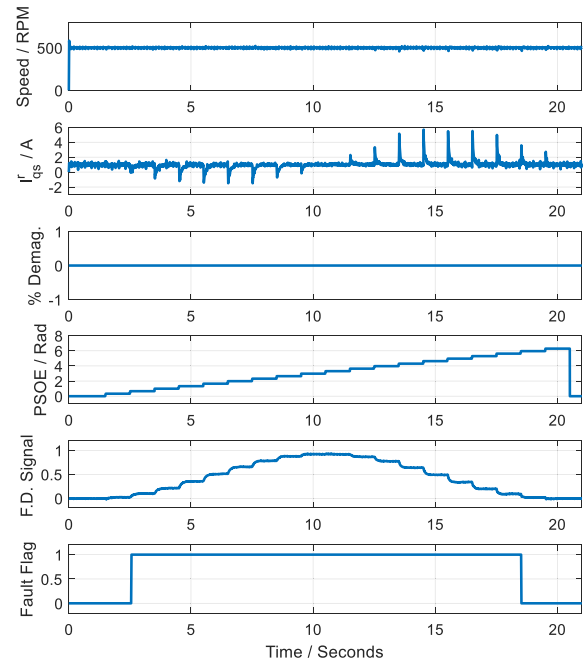


FIGURE 18. Experimental results on false positive uniform demagnetization caused by PSOE.

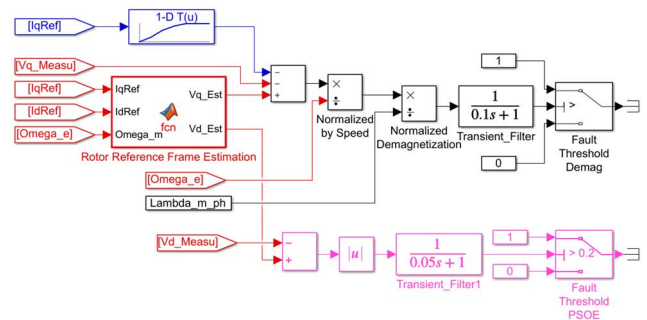


FIGURE 19. Improved demagnetization detection with PSOE disambiguation.

TABLE 2. Fault flag interpretation.

Fault Type	Demagnetization Fault Flag (>5%)	PSOE Fault Flag (>0.3rad)
No Fault	0	0
Demagnetization Fault	1	0
PSOE Fault	1	1

is method is summarized in Table 2. The direct axis voltage error is filtered and compared with a set threshold for the second flag. Therefore, when a PSOE is introduced to the system, both demagnetization detection flag and PSOE fault flag will be set. Fault disambiguation algorithm in flow chart form is shown in figure 20.

Figure 11 ($t > 5$ seconds) shows simulation results on the disambiguation strategy. Results shown in figures 21 through 25 experimentally demonstrate the operation of the proposed demagnetization detection and disambiguation at various

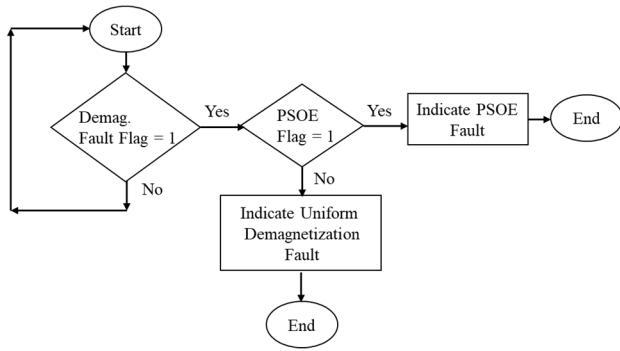


FIGURE 20. Fault disambiguation algorithm flow chart.

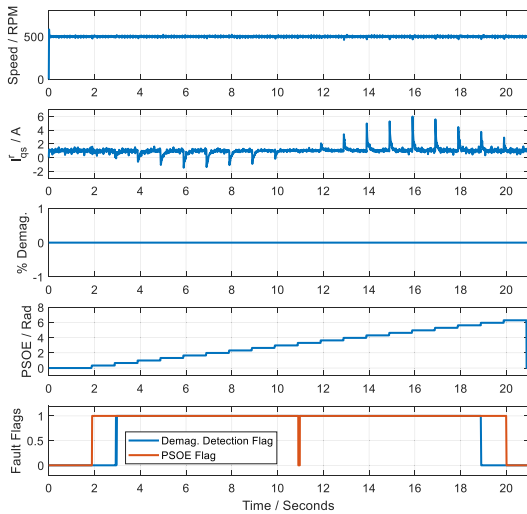


FIGURE 21. Experimental results on the improved demagnetization detection with PSOE disambiguation (500 RPM, $I_{qs}^* = 1$ A).

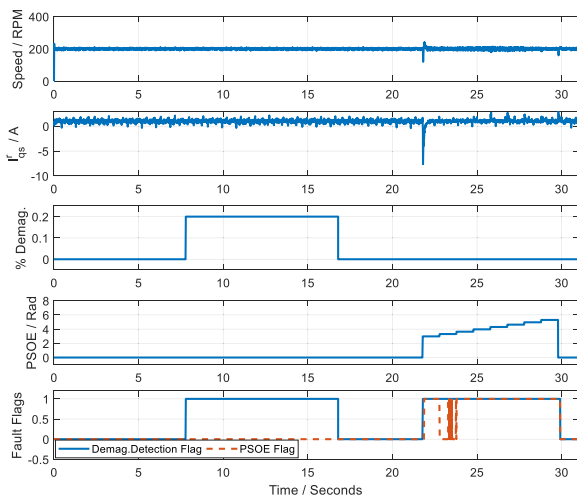


FIGURE 22. Experimental results on the improved demagnetization detection with PSOE disambiguation (200 RPM, $I_{qs}^* = 1$ A).

speed and current references. Figure 21 subplot 4 indicates the injection of PSOE with fifth subplot indicating the behavior of the two flags enabling the disambiguation of a

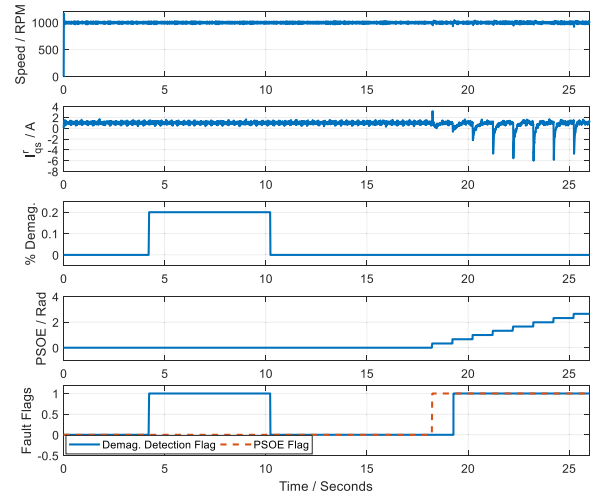


FIGURE 23. Experimental results on the improved demagnetization detection with PSOE disambiguation (1000 RPM, $I_{qs}^* = 1$ A).

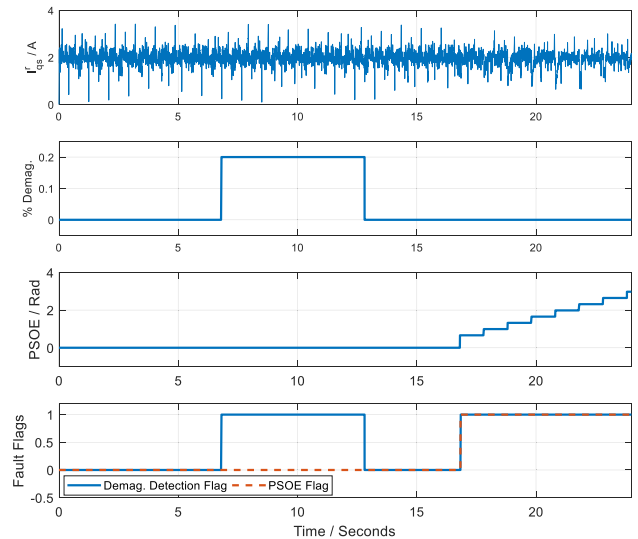


FIGURE 24. Experimental results on the improved demagnetization detection with PSOE disambiguation (200 RPM, $I_{qs}^* = 2$ A).

uniform demagnetization fault from a PSOE fault. Initially in figures 22 through 25, a demagnetization fault has been injected, and the fault is removed. Experiments are then continued by injecting a PSOE fault with varying error. In each test case the demagnetization detection flag is set when a demagnetization fault has been injected. Further, when a PSOE is injected, both the demagnetization detection flag and PSOE flag are being set. Table 2 is useful in interpreting these results. According to the table, demagnetization flag itself solely indicates a demagnetization fault. However, both demagnetization flag and PSOE flags indicate a PSOE fault, assisting in disambiguation between these two faults, justifying our claims (flow chart in figure 20). Digital filters and threshold selection are used to block potential false positives caused by transients. Therefore, the fault detection may not be possible for a minute range of the fault diagnosis signal,

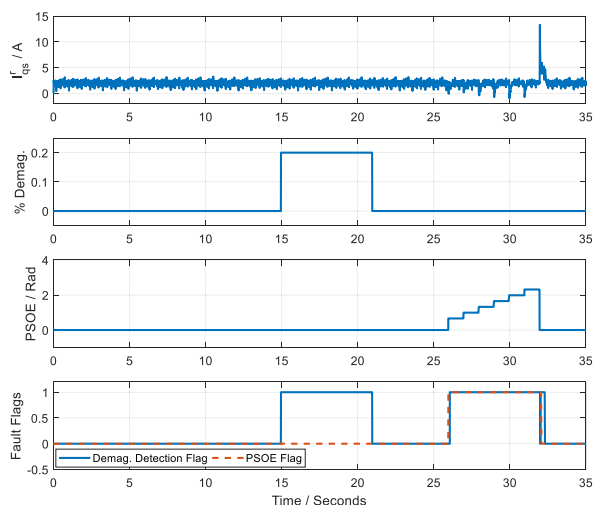


FIGURE 25. Experimental results on the improved demagnetization detection with PSOE disambiguation (500 RPM, $I_{qs}^* = 2$ A).

which is unavoidable and a limitation in the proposed disambiguation strategy.

VI. CONCLUSION

PMSMs are widely used in applications requiring high torque density and high dynamic controls. However, the magnets used in PMSM rotors, may experience uniform demagnetization under high operating temperature, extensive field weakening control or manufacturing defects. Such a failure can result in the machine to underperform in an application and endanger system functionality. Hence uniform demagnetization detection is advantageous in improving overall system performance. However, uniform demagnetization detection algorithms that rely on quadrature axis voltage is prone false positives under a position sensor offset error (PSOE), which is another crucial fault itself. Further, unlike the demagnetization fault, a PSOE can be easily compensated without removing the motor. Hence disambiguation of the fault is of paramount importance. This paper proposes a simple strategy to disambiguate the two faults through a time domain signal-based approach. The proposed algorithm has been verified with simulation, and experimental results at multiple operating points and transient states, validating the approach.

REFERENCES

- [1] J. Faiz and E. Mazaheri-Tehrani, "Demagnetization modeling and fault diagnosing techniques in permanent magnet machines under stationary and nonstationary conditions: An overview," *IEEE Trans. Ind. Appl.*, vol. 53, no. 3, pp. 2772–2785, May/June 2017, doi: [10.1109/TIA.2016.2608950](https://doi.org/10.1109/TIA.2016.2608950).
- [2] Z. Mynar, L. Vesely, and P. Vaclavek, "PMSM model predictive control with field-weakening implementation," *IEEE Trans. Ind. Electron.*, vol. 63, no. 8, pp. 5156–5166, Aug. 2016, doi: [10.1109/TIE.2016.2558165](https://doi.org/10.1109/TIE.2016.2558165).
- [3] S. Chi, Z. Zhang, and L. Xu, "Sliding-mode sensorless control of direct-drive PM synchronous motors for washing machine applications," *IEEE Trans. Ind. Appl.*, vol. 45, no. 2, pp. 582–590, Mar. 2009, doi: [10.1109/TIA.2009.2013545](https://doi.org/10.1109/TIA.2009.2013545).
- [4] T. Sebastian, "Temperature effects on torque production and efficiency of PM motors using NdFeB magnets," *IEEE Trans. Ind. Appl.*, vol. 31, no. 2, pp. 353–357, Mar./Apr. 1995, doi: [10.1109/28.370284](https://doi.org/10.1109/28.370284).
- [5] A. Sarikhani and O. Mohammed, "Real-time demagnetization assessment of PM synchronous machine," in *Proc. 20th Int. Conf. Electr. Mach.*, Sep. 2012, pp. 2418–2424, doi: [10.1109/ICELMach.2012.6350222](https://doi.org/10.1109/ICELMach.2012.6350222).
- [6] J. Zhao, L. Wang, L. Xu, F. Dong, J. Song, and X. Yang, "Uniform demagnetization diagnosis for permanent-magnet synchronous linear motor using a sliding-mode velocity controller and an ALN-MRAS flux observer," *IEEE Trans. Ind. Electron.*, vol. 69, no. 1, pp. 890–899, Jan. 2022, doi: [10.1109/TIE.2021.3050360](https://doi.org/10.1109/TIE.2021.3050360).
- [7] Y. Gritli, A. Tani, C. Rossi, and D. Casadei, "Detection of rotor magnet demagnetization in asymmetrical six-phase surface mounted permanent magnet synchronous motor drive," in *Proc. 13th Int. Conf. Electr. Mach. (ICEM)*, Sep. 2018, pp. 1809–1814, doi: [10.1109/ICELMACH.2018.8506688](https://doi.org/10.1109/ICELMACH.2018.8506688).
- [8] K. Ahsanullah, E. Jeyasankar, S. K. Panda, R. Shanmukha, and S. Nadarajan, "Detection and analysis of winding and demagnetization faults in PMSM based marine propulsion motors," in *Proc. IEEE Int. Electric Mach. Drives Conf. (IEMDC)*, May 2017, pp. 1–7, doi: [10.1109/IEMDC.2017.8002050](https://doi.org/10.1109/IEMDC.2017.8002050).
- [9] J. Hong, S. Park, D. Hyun, T. J. Kang, S. B. Lee, C. Kral, and A. Haumer, "Detection and classification of rotor demagnetization and eccentricity faults for PM synchronous motors," *IEEE Trans. Ind. Appl.*, vol. 48, no. 3, pp. 923–932, May/June 2012, doi: [10.1109/TIA.2012.2191253](https://doi.org/10.1109/TIA.2012.2191253).
- [10] J.-R. R. Ruiz, J. A. Rosero, A. G. Espinosa, and L. Romeral, "Detection of demagnetization faults in permanent-magnet synchronous motors under nonstationary conditions," *IEEE Trans. Magn.*, vol. 45, no. 7, pp. 2961–2969, Jul. 2009, doi: [10.1109/TMAG.2009.2015942](https://doi.org/10.1109/TMAG.2009.2015942).
- [11] S. Rajagopalan, J. M. Aller, J. A. Restrepo, T. G. Habetler, and R. G. Harley, "Detection of rotor faults in brushless DC motors operating under nonstationary conditions," *IEEE Trans. Ind. Appl.*, vol. 42, no. 6, pp. 1464–1477, Nov./Dec. 2006, doi: [10.1109/TIA.2006.882613](https://doi.org/10.1109/TIA.2006.882613).
- [12] M. Zafarani, T. Goktas, and B. Akin, "A comprehensive magnet defect fault analysis of permanent-magnet synchronous motors," *IEEE Trans. Ind. Appl.*, vol. 52, no. 2, pp. 1331–1339, Mar./Apr. 2016, doi: [10.1109/TIA.2015.2487440](https://doi.org/10.1109/TIA.2015.2487440).
- [13] J. Faiz and H. Nejadi-Koti, "Demagnetization fault indexes in permanent magnet synchronous motors—An overview," *IEEE Trans. Magn.*, vol. 52, no. 4, pp. 1–11, Apr. 2016, doi: [10.1109/TMAG.2015.2480379](https://doi.org/10.1109/TMAG.2015.2480379).
- [14] T. Goktas, M. Zafarani, K. W. Lee, B. Akin, and T. Sculley, "Comprehensive analysis of magnet defect fault monitoring through leakage flux," *IEEE Trans. Magn.*, vol. 53, no. 4, pp. 1–10, Apr. 2017, doi: [10.1109/TMAG.2016.2617318](https://doi.org/10.1109/TMAG.2016.2617318).
- [15] M. Zhu, W. Hu, and N. C. Kar, "Acoustic noise-based uniform permanent-magnet demagnetization detection in SPMSM for high-performance PMSM drive," *IEEE Trans. Transport. Electric.*, vol. 4, no. 1, pp. 303–313, Mar. 2018, doi: [10.1109/TTE.2017.2755549](https://doi.org/10.1109/TTE.2017.2755549).
- [16] M. Zhu, W. Hu, and N. C. Kar, "Multi-sensor fusion-based permanent magnet demagnetization detection in permanent magnet synchronous machines," *IEEE Trans. Magn.*, vol. 54, no. 11, pp. 1–6, Nov. 2018, doi: [10.1109/TMAG.2018.2836182](https://doi.org/10.1109/TMAG.2018.2836182).
- [17] M. S. Rafiq, H. Lee, Y. Park, S.-B. Lee, M. O. Zapico, D. Fernandez, D. Diaz-Reigosa, and F. Briz, "Airgap search coil based identification of PM synchronous motor defects," *IEEE Trans. Ind. Electron.*, vol. 69, no. 7, pp. 6551–6560, Jul. 2022, doi: [10.1109/TIE.2021.3095810](https://doi.org/10.1109/TIE.2021.3095810).
- [18] H. Chen, C. Gao, J. Si, Y. Nie, and Y. Hu, "A novel method for diagnosing demagnetization fault in PMSM using toroidal-yoke-type search coil," *IEEE Trans. Instrum. Meas.*, vol. 71, pp. 1–12, 2022, doi: [10.1109/TIM.2021.3134991](https://doi.org/10.1109/TIM.2021.3134991).
- [19] C. Zeng, S. Huang, J. Lei, Z. Wan, and Y. Yang, "Online rotor fault diagnosis of permanent magnet synchronous motors based on stator tooth flux," *IEEE Trans. Ind. Appl.*, vol. 57, no. 3, pp. 2366–2377, May 2021, doi: [10.1109/TIA.2021.3058541](https://doi.org/10.1109/TIA.2021.3058541).
- [20] M. Skowron, T. Orlowska-Kowalska, and C. T. Kowalski, "Detection of permanent magnet damage of PMSM drive based on direct analysis of the stator phase currents using convolutional neural network," *IEEE Trans. Ind. Electron.*, vol. 69, no. 12, pp. 13665–13675, Dec. 2022, doi: [10.1109/TIE.2022.3146557](https://doi.org/10.1109/TIE.2022.3146557).
- [21] S. S. Kuruppu, "Position sensor harmonics influence on highly integrated field oriented controlled PMSM drive torque output," in *Proc. IEEE Transp. Electric. Conf. Expo (ITEC)*, Jun. 2021, pp. 427–433.
- [22] S. S. Kuruppu and Y. Zou, "Static position sensor bias fault diagnosis in permanent magnet synchronous machines via current estimation," *IEEE/ASME Trans. Mechatronics*, vol. 26, no. 2, pp. 888–896, Apr. 2021, doi: [10.1109/TMECH.2020.3010898](https://doi.org/10.1109/TMECH.2020.3010898).

- [23] S. S. Kuruppu and Y. Zou, "Post production PMSM position sensor offset error quantification via voltage estimation," in *Proc. IEEE Energy Convers. Congr. Exposit. (ECCE)*, Oct. 2020, pp. 3355–3361, doi: 10.1109/ECCE44975.2020.9235757.



SANDUN S. KURUPPU (Senior Member, IEEE) received the B.S. degree in electrical and electronics engineering from the University of Peradeniya, Sri Lanka, in 2007, and the M.S. and Ph.D. degrees from Purdue University, West Lafayette, IN, USA, in 2010 and 2013, respectively.

He is currently an Associate Professor in electrical and computer engineering at Saginaw Valley State University (SVSU), MI, USA. Prior to his current position, he was with Nexteer Automotive,

Texas Instruments Kilby Laboratories, and Delphi Electronics and Safety. His current research interests include fault prognostics, diagnostics, localization, mitigation in mechatronic systems, power electronics, vehicle stability control, and extremum seeking controls for traction applications.

Dr. Kuruppu was a recipient of Ruth and Ted Braun Fellowship and Award for Excellence for Online Teaching at SVSU, in 2021. He is an Associate Editor of IEEE Power Electronics Society, Educational Videos on Power Electronics, and the Student Activities Chair of IEEE ECCE 2022.



SUNIL G. ABEYRATNE (Senior Member, IEEE) was born in Kandy, Sri Lanka. He received the B.Sc. (Eng.) degree in electrical and electronics engineering from the University of Peradeniya, Peradeniya, Sri Lanka, in 1987, and the M.Eng. and Ph.D. degrees from Gifu University, Gifu, Japan, in 1992 and 1997, respectively.

From 1987 to 1988, he was an Instructor with the Department of Electrical and Electronic Engineering, University of Peradeniya.

In 1998, he joined the Colombo Dockyard Ltd., as an Electrical and Electronic Engineer, and worked, until January 2000. He was a Researcher with the Wisconsin Power Electronics Research Center, University of Wisconsin–Madison, Madison, WI, USA, from 1992 to 1994. From 1997 to 1998, he was a Software Engineer with Total Office O, Japan. He joined the University of Peradeniya as a Senior Lecturer, in 1999. He was with Toshiba Schneider Inverter Corporation, Design and Development Group, Mie, Japan, as a Researcher/a Trainee, in 2001. Since 2017, he has been a Professor with the Faculty of Engineering, University of Peradeniya.

• • •